Title

THEORY OF COULOMB-NUCLEAR INTERFERENCE FOR HEAVY-ION EXCITATION OF ROTATIONAL STATES

Author

Guidry, M.W.

Publication Date

1976

Submitted to Nuclear Physics A

LBL-4357
Preprint

THEORY OF COULOMB-NUCLEAR INTERFERENCE FOR HEAVY-ION EXCITATION OF ROTATIONAL STATES

M. W. Guidry, H. Massmann, R. Donangelo, and
J. O. Rasmussen

January 1976

Prepared for the U. S. Energy Research and
Development Administration under Contract W-7405-ENG-48

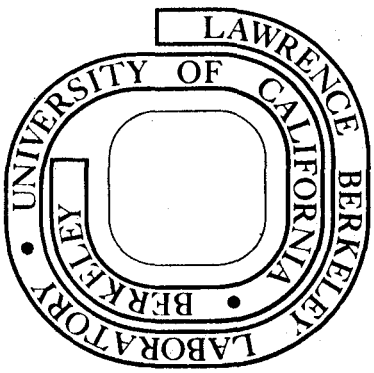

DISCLAIMER

LBL-4357

THEORY OF COULOMB-NUCLEAR INTERFERENCE FOR HEAVY-ION EXCITATION OF ROTATIONAL STATES

M. W. Guidry, H. Massmann, † R. Donangelo, and J. O. Rasmussen

Lawrence Berkeley Laboratory*
University of California
Berkeley, California 94720

ABSTRACT

The Uniform Semiclassical Approximation (USCA) with complex trajectories is applied to the problem of Coulomb-nuclear interference for rotational states excited in heavy-ion reactions. The system $^{40}Ar + ^{238}U$ is studied as a function bombarding energy. The calculations show considerable sensitivity of the excitation probabilities to both the real and imaginary parts of the complex nuclear potential in the vicinity of the Coulomb barrier, suggesting that heavy-ion rotational excitation could be a sensitive probe of the nuclear potential near the barrier in deformed nuclei.

I. INTRODUCTION

The phenomenon of Coulomb-nuclear interference has been extensively studied for rotational excitation with light ions, [1-8] and vibrational excitation with heavier projectiles.[9-13] The nature of this effect for heavy-ion rotational excitation has received little attention (see, however, refs. 14-16).

The shortness of the deBroglie wavelength associated with heavy-ion projectiles implies that classical or semiclassical methods may be feasible for the investigation of heavy-ion Coulomb-nuclear interference. The recent assimilation into nuclear physics of uniform semiclassical methods[17-24] originally developed in the theory of molecular scattering[25-36] provides a promising vehicle for such calculations. The underlying idea of these methods is that one uses analytical continuation of the classical equations of motion for the description of the dynamics of the system, together with quantized boundary conditions and the quantum-mechanical superposition principle in adding amplitudes for different trajectories leading to the same final state.

These new techniques have several advantages relative to the earlier semiclassical methods:[37,38] 1) because one integrates exact classical equations of motion, the nucleus-projectile interaction is easily modified to include higher multipoles, different nuclear form factors, etc., the resulting formalism being dynamically exact in the classical limit; 2) the effect of the imaginary nuclear potential on the trajectory is included exactly rather than as a first-order mean free path absorption; 3) the results may be interpreted in terms of classical concepts, albeit with complex trajectories.

A disadvantage is that the method is obviously restricted to cases in which a classical model can be formulated to describe the system. In Part II a brief description of the theory is given and in Part III we discuss the general effect of the complex potential on the rotational excitation probabilities. Part IV deals with a realistic example, $^{40}Ar + ^{238}U$, for bombarding energies in the range E_{lab} = 150 - 220 MeV. Conclusions are presented in Part V.

II. BASIC THEORY

We are concerned here with generalizing the USCA theory of Coulomb excitation presented in ref. 23 to include a deformed complex optical potential. The fundamental quantities to be determined will be the probability amplitudes and phases for excitation in the channels of interest. These represent components of the quantum-mechanical S-matrix evaluated by saddle-point (stationary phase) integration methods.[18,19)]

We will restrict ourselves to the case of a head-on collision, since then the motion is confined to a plane, which simplifies the numerical calculation. The generalization to a three-dimensional rotor will be made subsequently by arguments similar to those used previously for pure Coulomb excitation.[23,24)] The coordinate system and relevant parameters are illustrated in Fig. 1. In the present paper we confine ourselves to interactions at or below the Coulomb barrier. Then the Hamiltonian describing the system is parameterized by the form

$$\mathcal{H} = \frac{P_r^2}{2m} + P_\chi^2\left(\frac{1}{mr^2} + \frac{1}{2\mathcal{J}}\right) + \frac{Z_p Z_t e^2}{r} + \frac{Z_p e^2}{2r^3}\, Q_0^{(2)}\, P_2(\cos\chi)$$

$$+ \frac{Z_p e^2}{2r^5}\, Q_0^{(4)}\, P_4(\cos\chi) - V f_r - iW f_I \qquad (1)$$

with

$$f_R = \left[1 + \exp\left(\frac{r - R_R}{a_R}\right)\right]^{-1}$$
$$\qquad (2)$$
$$f_I = \left[1 + \exp\left(\frac{r - R_I}{a_I}\right)\right]^{-1}$$

where m is the reduced mass of the system, r is the radial coordinate, $\chi = (\beta - \theta)$ is the angle between the symmetry axis of the rotor and the line joining the centers of the target and projectile, $P_\lambda(\cos\chi)$ is a Legendre polynomial, Z_p and Z_t are the charges of the projectile and target respectively, and P_r and P_χ are the classical radial and angular momenta conjugate to r and β. The multipole moments $Q_0^{(\lambda)}$ are defined by

$$Q_0^{(\lambda)} = \sqrt{\frac{16\pi}{2\lambda + 1}} \int d^3r\, \rho(r)\, Y_{\lambda 0}(\underset{\sim}{r}) r^\lambda \qquad (3)$$

where λ is the multipole order, $\rho(r)$ is the target nucleus charge-density function, and $Y_{\lambda 0}(\underset{\sim}{r})$ is a spherical harmonic. The moment of inertia $\mathcal{J}$ is taken for the present calculation from the experimental excitation energy of the first 2^+ state of the rotor. The nuclear interaction is parameterized in terms of a complex optical potential with different Woods-Saxon form factors for the real potential V and the imaginary potential W. The diffuseness parameters for the real and imaginary potentials are denoted by a_R and a_I respectively, and the real radius is

$$R_R = R_0^R \left[A_p^{1/3} + A_t^{1/3} \left(1 + \beta_2 Y_{20}(\chi) + \beta_4 Y_{40}(\chi) - \frac{\beta_2^2 + \beta_4^2}{4\pi} \right) \right] \quad (4)$$

where R_0^R is the real optical radius, A_p and A_t are the projectile and target masses respectively, and the β_λ are the nuclear deformation parameters. The last term conserves volume to this order in the deformation parameters. For the present work the real and the imaginary potentials are assumed to have different radial geometry but the same angular dependence, and the imaginary radius R_I is defined by replacing R_0^R with its counterpart R_0^I in Eq. (4).

For a purely real nuclear potential and for $Q_0^{(4)} = 0$, the model for Coulomb-nuclear interference is thus conceived as a competition between the repulsive electric quadrupole force and the attractive real nuclear force in imparting net torque to the deformed rotor, as Fig. 2 illustrates. The inclusion of the hexadecapole potential and the imaginary nuclear potential complicates this simple picture, but the classical model remains one of a competition between the contributions of attractive and repulsive parts of the total potential to the net torque of the system.

From the Hamiltonian (1) the classical equations of motion are

$$\dot{r} = \frac{p_r}{m} \quad (5a)$$

$$\dot{\chi} = \left(\frac{1}{mr^2} + \frac{1}{\mathcal{I}} \right) P_\chi \quad (5b)$$

$$\dot{P}_r = \frac{P_\chi^2}{mr^3} + \frac{Z_p Z_t e^2}{r^2} + \frac{3}{2} \frac{Z_p e^2 Q_0^{(2)}}{r^4} P_2(\cos\chi) + \frac{5}{2} \frac{Z_p e^2 Q_0^{(4)}}{r^6} P_4(\cos\chi) - V \frac{\partial f_R}{\partial r} - iW \frac{\partial f_I}{\partial r} \quad (5c)$$

$$\dot{P}_\chi = -\frac{Z_p e^2 Q_0^{(2)}}{2r^3}\frac{\partial}{\partial\chi}[P_2(\cos\chi)] - \frac{Z_p e^2 Q_0^{(4)}}{2r^5}\frac{\partial}{\partial\chi}[P_4(\cos\chi)]$$

$$+ V\frac{\partial f_R}{\partial\chi} + iW\frac{\partial f_I}{\partial\chi} \qquad (5d)$$

In addition, the classical action Φ in units of $\hbar$ is determined from

$$\dot{\Phi} = -\frac{1}{\hbar}(r\dot{P}_r + \chi\dot{P}_\chi) \qquad (5e)$$

We will confine ourselves to the incoming $\ell = 0$ partial wave. Then classically the projectile is incident on the target with zero impact parameter and the initial conditions for the integration of the classical equations of motion are

$$r_i = \text{large and real} \qquad (6a)$$

$$P_{r_i} = \sqrt{2m\left(E_{CM} - \frac{Z_p Z_t e^2}{r_i}\right)} \qquad (6b)$$

$$\chi_i = \beta_0 \text{ (arbitrary and complex)} \qquad (6c)$$

$$P_{\chi_i} = 0 \qquad (6d)$$

$$\Phi_i = 0 \qquad (6e)$$

The trajectories during the integration are complex due to the complex nuclear potential and due to the fact that β_0 may in general be complex. Following the integration, observable quantities must be real. This may be specified for P_χ by appropriate choice of the imaginary part of the initial orientation β_0, and is then assured for P_r by virtue of the time-independent Hamiltonian. Finally r may be made real by selection of an appropriate complex time path in the asymptotic region of the integration as in ref. 31.

Integration of the complex equations of motion leads to the extension into the complex plane of the classical rotational angular momentum quantum-number function discussed in ref. 23:

$$\hat{I}_f(\beta_0) = P_\chi(\beta_0)/\hbar \tag{7}$$

The final spin $I_f(\beta_0)$ has a real and imaginary part, each of which is a function of a complex variable β_0. The roots analogous to those specified in ref. 23 must satisfy the criteria

$$\mathrm{Re}[\hat{I}_f(\beta_0)] = \text{even integer} + \tfrac{1}{2} \tag{8a}$$

$$\mathrm{Im}[\hat{I}_f(\beta_0)] = 0 \tag{8b}$$

This is accomplished by appropriate choice of the complex initial orientation β_0; (see Fig. 5 for an approximate graphical solution to Eq. 8a).

For the cases studied here one or two complex trajectories make the dominant contribution to the two-dimensional S-matrix. For two contributing trajectories the uniform semiclassical S-matrix describing the rotational excitation of the target to a final angular momentum I is given by:[34]

$$S_{I\leftarrow 0}(E) = -\sqrt{\pi}\, e^{i/2(\Phi_1+\Phi_2)} \left\{ (\sqrt{\bar{p}_1} + \sqrt{-\bar{p}_2})^{\frac{1}{4}}\, \mathrm{Ai}(-\xi) + (-i)(\sqrt{\bar{p}_1} - \sqrt{-\bar{p}_2})\, \frac{1}{\xi^{\frac{1}{4}}}\, \mathrm{Ai}'(-\xi) \right\} \tag{9}$$

where the subscripts 1 and 2 refer to the classical trajectories which satisfy the boundary conditions of Eq. (8). The amplitudes $\bar{p}_j$ are defined by[23]

$$\bar{p}_j = \frac{2\sin\bar{\beta}_j}{\left(\dfrac{\partial \hat{I}(\bar{\beta}_j)}{\partial \bar{\beta}_j}\right)} \qquad \left(\bar{\beta}_j \equiv (\bar{\beta}_0)_j;\ j = 1,2\right) \tag{10}$$

The $\sin\bar{\beta}_j$ factor is the analogue of the weighting factor used in ref. 23 to make the transition from a two-dimensional to a three-dimensional rotor. In general, $\sin\bar{\beta}_j$ and the derivative in Eq. (10) are complex. The function ξ is defined by

$$\xi = [3/4(\Phi_2 - \Phi_1)]^{2/3} = [3/4\ \Delta\Phi]^{2/3} \tag{11}$$

and Ai and Ai' are respectively the complex regular Airy function and its derivative. The trajectory subindex $j = 2$ is the one for which $\mathrm{Re}(\partial\hat{I}(\bar{\beta})/\partial\bar{\beta}) < 0$. The excitation probability $P_{I\leftarrow 0}$ is given by

$$P_{I\leftarrow 0}(E) = |S_{I\leftarrow 0}(E)|^2 \tag{12}$$

For the case that $|\Delta\Phi| \gg 1$ one can use the asymptotic expressions for the Airy functions to obtain the "primitive" excitation probability, which is useful because of its conceptual simplicity:

$$P^{\mathrm{prim}}_{I\leftarrow 0} = |\bar{p}_1|\, e^{-2\mathrm{Im}(\Phi_1)} + |\bar{p}_2|\, e^{-2\mathrm{Im}(\Phi_2)} + 2e^{\frac{1}{2}\mathrm{Im}(\Phi_1 + \Phi_2)} \sqrt{|\bar{p}_1\bar{p}_2|}\, \sin(\mathrm{Re}(\Delta\Phi) + \alpha) \tag{13-a}$$

"allowed transitions"

$$P^{\mathrm{prim}}_{I\leftarrow 0} = e^{-2\mathrm{Im}\Phi}\, |\bar{p}| \tag{13-b}$$

"forbidden transitions"

where α is the phase of $-\bar{p}_1\bar{p}_2{}^*$. For pure Coulomb excitation $\alpha = 0$.[23] As long as the nuclear force does not dominate (which is generally true in the present case for bombarding energies below the Coulomb barrier) α will be small and

can be neglected when Eq. (13) is used for qualitative considerations. Equation (13) is of use in illustrating two important concepts: 1) the interference between the amplitudes arising from the different terms in the S-matrix, and 2) the exponential damping of the probability amplitudes by the imaginary part of the classical action Φ. For the numerical calculation, however, the uniform expression (9) was used.

Finally, we note that the imaginary potential erases the strict distinction found in Coulomb excitation[23] between the allowed states (those states reached by purely real trajectories) and forbidden states (those states reached only by complex trajectories). With an imaginary potential all trajectories will generally be complex. However, for imaginary potentials which are not too large it is permissible to speak of 'allowed' states ($\mathrm{Im}\beta_0 \approx 0$) and 'forbidden' states ($|\mathrm{Im}\beta_0| \gg 0$). The former will be largely characterized by interference between two contributing trajectories, while the dominant feature of the latter will be an exponential damping of the probability for a single contributing trajectory, as a consequence of the penetration of the projectile into classically inaccessible regions.

III. THE GENERAL EFFECT OF THE NUCLEAR FORCE ON THE ROTATIONAL EXCITATION PROBABILITIES

The four potential parameter sets for the nuclear Hamiltonian (1) that have been studied are displayed in Table 1. The Coulomb and deformation parameters are from refs. 40 and 41. The nuclear parameters are taken from quasi-elastic scattering of $^{84}Kr + ^{208}Pb$ at E_{lab} = 450 MeV (set II)[42] and $^{40}Ar + ^{238}U$ at E_{lab} = 286 MeV (sets III and IV).[43] We emphasize that there are reservations about the propriety of these potentials for the application discussed here since our calculations are for lower energies than where they were determined, and for the other reasons mentioned below. Nevertheless, these potentials still serve as useful starting points for the investigation of rotational scattering in the barrier region.

In Fig. 3 the real and imaginary parts of the Coulomb and nuclear potentials along the symmetry axis of the target are plotted as a function of the real part of the radial coordinate r. Caution should be exercised in referring to Fig. 3. Since the trajectory is in general complex, one must consider not just the potential on the real r axis, but the potential along the entire trajectory in the complex r-plane.[39] Nevertheless, for energies where Wf_I in Eq. (1) is not too large, and when $Im(\beta_0) \approx 0$, the r trajectory is nearly real and Fig. 3 is a useful approximation to the potentials encountered on the complex classical trajectories.

The model of competition among the repulsive and attractive forces in the nuclear Hamiltonian is clearly illustrated in Fig. 4 where we have plotted the classical angular momentum $I = P_\chi/\hbar$ as a function of time during the interaction for a given initial orientation and several different projectile energies. With increasing energy there is a cancellation of the angular momentum imparted by the non-central repulsive

potential until finally the attractive nuclear potential dominates and the direction of the rotation is completely reversed from that of pure Coulomb excitation. This is further illustrated in Fig. 5 where the real part of the quantum number function (final spin vs. initial orientation) is plotted with and without the nuclear potential (set II). The final spin is lowered by the action of the nuclear force. Graphical solutions of (8-a) for the limit β_0 real are indicated for the Coulomb excitation case and for the Coulomb-nuclear case.

The phase difference $\Delta\Phi$ is much more sensitive to the details of the interaction on a particular trajectory than the classical angular momentum. Therefore the interference term of Eq. (14), which is proportional to $\sin[\mathrm{Re}(\Delta\Phi)]$, will be a more delicate probe of the competition between nuclear and Coulomb forces in the interaction region. This is illustrated in Fig. 6 where excitation probabilities for 180-MeV ^{40}Ar on ^{238}U are plotted with and without the complex nuclear potential (set II). This energy is some 40 MeV below the classical barrier for spherical nuclei, but the effect of the nuclear potential on the excitation probabilities is as large as 50-100% (note the logarithmic scale). These results can be largely understood in terms of the effect of the nuclear interaction on the real part of the phase difference $\Delta\Phi$ in Eq. (13). In Fig. 7 the value of $\mathrm{Re}(\Delta\Phi)$ as a function of final spin is plotted, with the constructive and destructive regions for the interference term of Eq. (13) indicated. Taking the 4^+ state as an example, we note that relative to the case of pure Coulomb excitation, the nuclear potential shifts the interference term of Eq. (13) further into a region of destructive interference, thus decreasing the excitation probability of the 4^+ state relative to that of pure Coulomb excitation. Also plotted are the excitation amplitudes, but at this energy the significant

change in the excitation probability is due to the change in the phase. Similarly, the phase difference for the 6^+ state is shifted from a region of destructive interference to one where the interference term is essentially zero. Therefore the excitation probability is increased for the 6^+ state relative to the case of pure Coulomb excitation. The behavior of the other probabilities for $I^\pi \lesssim 8^+$ is understood in a like manner. As discussed further below, and as Fig. 7 indicates, the nuclear force also lowers the probability amplitudes significantly for the higher-spin states ($I^\pi \geqslant 8^+$), in addition to affecting the phase.

The effect of the nuclear potential is further illustrated in Fig. 8, where the real part of the phase difference is plotted as a function of energy for several states with and without the nuclear potential. For a given state, the passage of $\Delta\Phi$ through regions of constructive and destructive interference is primarily responsible for the well-known oscillations in Coulomb excitation probabilities as a function of energy.[23] The effect of the real nuclear potential is to shift the phase difference further below its value for pure Coulomb excitation with increasing energy. In extreme cases the interference term may be shifted from a constructive maximum to a destructive minimum at a given energy, or vice-versa. With increasing energy (or for high-spin states) the effect of the nuclear force on the probability amplitudes $\sqrt{\bar{p}_j}$ also becomes significant. This is a consequence of the effect of the lowered quantum-number function (cf. Fig. 5) on the derivatives in Eq. (10). Until the region where the nuclear force dominates, the general effect of increasing energy is to increase the probability amplitudes of the lower-spin states relative to that of the very high-spin states. This is a direct reflection of the competition between repulsive and attractive forces in producing torque, and has been observed previously.[16] Note, however, that this concentration of *probability amplitudes* in lower spins does not necessarily manifest itself in a concentration of *probability* in a particular lower-spin state as it would

in a purely classical model. The contribution from the interference term of Eq. (13) must also be considered as a function of energy.

The sensitivity to the potential parameters is further illustrated in Fig. 9 where we have plotted for a purely real potential the variation of some rotational state excitation probabilities as a function of the real radius parameter R_0^R. Note that even a small change in R_0^R produces large changes in the probabilities, and that the behavior of the probabilities as a function of R_0^R is very different for each state. For example, if R_0 = 1.21 fm, a 0.5% decrease in R_0 results in changes of -10%, +10%, -10%, -7%, +2%, -6%, and +12% for the 0^+-12^+ state probabilities respectively. These changes can be explained, as have the previous examples, in terms of the nuclear-force influence on the phase differences $\Delta\Phi$ and the amplitudes $\sqrt{\bar{p}_j}$.

The probabilities should also be sensitive to the imaginary potential for two reasons: 1) absorption due to the imaginary potential may destroy the interference term in Eq. (13) by preferentially absorbing one of the trajectories, setting $\bar{p}_1$ or $\bar{p}_2 = 0$, and 2) because the equations of motion are complex, the trajectory of the projectile is affected by the imaginary potential.

For a small value of Wf_I, the primary effect of the imaginary potential on the probability amplitudes is to contribute a damping factor $e^{-Im\Phi}$ which is given approximately by[38]

$$e^{-Im\Phi} \approx e^{-W\int f_I(t)dt} \tag{14}$$

where $f_I(t)$ is the form factor of the imaginary potential. In Fig. 10 the value of $Wf_I(t)$ as a function of t is plotted for several different initial orientations. From (14) the damping of the probability amplitudes

varies exponentially with the area under the curves. Obviously those initial orientations near 0° will be subject to stronger damping than those near 90°, and in the general case one of the probability amplitudes of Eq. (13) will be damped out before the other, destroying the oscillatory interference term.

In addition to absorption effects, the imaginary potential also affects the classical trajectory. This can give rise to reflection and diffraction phenomena not adequately treated in older semiclassical methods which only include the effect of the real potential on the projectile trajectory. Within the classical-limit framework described here, these effects are treated exactly, and the excitation probabilities should be sensitive to the imaginary as well as the real part of the complex nuclear potential in the sub-barrier region. In the next section we will further illustrate this sensitivity with some realistic calculations for a representative heavy-ion system.

IV. EXAMPLES AND DISCUSSION

We have applied the techniques described in the previous sections to the rotational excitation probabilities for the system $^{40}Ar + ^{238}U$. As before, the calculations were restricted to zero impact parameter. The excitation probabilities for the ground band were calculated for $I^{\pi} = 0^{+} - 12^{+}$ with the four potential parameter sets of Table 1 in the energy range E_{lab} = 150-220 MeV. The results are plotted in Figs. 11 and 12.

Consider first the states for which $I^{\pi} \leq 8^{+}$. In contrast to the light-ion case where mostly destructive Coulomb-nuclear interference is observed for low spins,[1-8] these states exhibit a large variety of both constructive and destructive interferences. The exact structure of the

interference depends on the nuclear potential as Figs. 11 and 12 indicate. This behavior is easily understood in qualitative terms, as discussed in Section III. Consider, for example, the 0^+ probability calculated with and without the nuclear force of parameter set II (Fig. 11). In the range 150-180 MeV the nuclear force has only a slight effect. Both the probability calculated with and that calculated without the nuclear force decreases. The reason is apparent in Fig. 8. For both cases the phase difference $\mathrm{Re}(\Delta\Phi)$ moves from a region of constructive interference into a region of destructive interference, the third term of Eq. (13) becomes algebraically smaller, and the excitation probability is decreased. In the region 170-180 MeV the effect of the nuclear force (primarily the real part in this case) begins to decrease the phase difference between the contributing trajectories relative to the case of Coulomb excitation. Thus, at $E_{lab} \approx 185$, Fig. 8 indicates that the interference term of Eq. (13) is essentially zero for the Coulomb excitation case while it is destructive for the case with the nuclear force included. The nuclear-force case thus exhibits a dip below that for Coulomb excitation in this region. Similarly, near $E_{lab} = 200$-205 MeV, both phase differences move into constructive interference regions and both the Coulomb and Coulomb-nuclear probabilities exhibit maxima. The Coulomb-nuclear peak is sharper because the phase difference is changing much more rapidly for it with energy (cf. Fig. 8). It is higher because at this energy the real nuclear force begins to affect appreciably the probability amplitudes. Finally for $E_{lab} > 205$ MeV, the real nuclear force shifts the phase difference toward a destructive region and, most importantly, the imaginary potential begins to damp the probability amplitudes by contributions to the imaginary phase. The result is a precipitous decrease in the excitation probability at

$E_{lab} \approx 210$ MeV. The other curves in Figs. 11 and 12 for $I^{\pi} \leq 8^{+}$. can be understood in a similar manner, though the situation for parameter sets III and IV is more complicated because the deeper imaginary potential at higher energies deflects the projectile from the real r axis, giving rise to reflective, diffractive, and absorptive effects not present for real r.[39]

The general behavior of the probabilities for sets III and IV in Figs. 11 and 12 is a rather structureless fall-off for $E_{lab} \gtrsim 190$ MeV. This is a consequence of the damping effect of the imaginary potential which comes strongly into play for the parameter sets III and IV before it does for set II. Thus for all three nuclear potentials the shift of the real part of the phase difference is the major effect for $E_{lab} \lesssim 190$ MeV, but in the region 190-210 MeV set II is dominated by the real part of the potential, while sets III and IV exhibit a strong influence of the imaginary potential. Finally, for all potentials exponential damping is the generally dominant feature for $E_{lab} > 210$ MeV.

For $I \lesssim 8$ a significant amount of oscillatory character is present, while for $I \gtrsim 8$ the general behavior is a monotonic decrease of the Coulomb-nuclear case below that of Coulomb excitation. This is explicable in terms of the approximate distinction between "classically allowed" and "classically forbidden" processes, as discussed in Section II and ref. 23. For $Wf_I \approx 0$ these correspond respectively to states below and above the maximum of the real quantum number function in Fig. 5. The forbidden states are reached by analytical continuation of the quantum number function into the complex β_0-plane. As a consequence of the complex initial orientation angle in those cases, one finds that only one of the $\bar{P}_j$ in Eq. (13) contributes significantly,

and it is exponentially damped by the acquisition of imaginary phase on the complex trajectory.[23] Therefore there is no interference term for the forbidden states and their excitation functions are monotonic rather than oscillatory.

For the forbidden states the deviation of the Coulomb-nuclear probabilities from pure Coulomb excitation is a consequence of the nuclear force's effect on the contributing probability amplitude (see Fig. 7). These amplitudes for the forbidden states are extremely sensitive to the maximum of the quantum number function on the real β_0 axis (Fig. 5), since the lowering of this function increases exponentially the damping of the contributing amplitude for a forbidden state. This damping is a consequence, not of the imaginary potential, but of the projectile penetration into regions inaccessible to classical dynamics with purely real trajectories. If an imaginary potential is also present it contributes an additional component to the damping as discussed in the classically allowed cases.

From Figs. 11 and 12 it is obvious that potential II differs greatly from III and IV in its influence on the rotational excitation probabilities. This may not be of physical significance, since they were determined with different projectiles, at different energies relative to the barrier, and on spherical and deformed nuclei, respectively. We may even question whether any of the potentials discussed here are realistic in the sub-barrier region for a deformed nucleus since 1) they were determined from fits using spherical optical codes on data in which true elastic and many quasi-elastic processes are indistinguishable, 2) there are theoretical reasons to believe the shape of the imaginary potential may differ from that of the real potential for a deformed nucleus, and 3) the Woods-Saxon optical potential may not be the best parameterization of the sub-barrier nuclear interaction. These reservations are not of major significance for the purpose of this paper however. We

have merely used these representative potentials to demonstrate that rotational excitation is sensitive to the complex nuclear potential, and that experimental determination of rotational excitation probabilities with heavy ions could be used to explore quantitatively the interaction in the Coulomb-nuclear interference region.

The probabilities calculated using parameter sets III and IV do not differ by more than 10-20% from each other in the energy range considered here. This is not surprising, since they were derived from fits to the same data, and Fig. 3 indicates that they are very similar in the critical region $Re(r) \gtrsim 13.5$ fm where most rotational excitation takes place at these projectile energies. Even in this case, however, the 10-20% differences for the large number of different states that are excited might allow some distinction between III and IV in a careful experiment.

V. CONCLUSIONS

We have demonstrated that rotational excitation probabilities in the Coulomb-nuclear interference region should be extremely sensitive to the details of the complex nuclear potential near the barrier. Both constructive and destructive Coulomb-nuclear interference is predicted if the imaginary potential is not too strong in the surface region. These effects are easily understood in terms of a simple classical model which describes competition between the electromagnetic and nuclear forces in producing rotational torque, and most importantly, the effect of the interaction on a sensitive phase difference between trajectories contributing to a particular state.

Because the excitation probabilities are sensitive to Coulomb-nuclear interference effects, we believe that heavy-ion rotational excitation patterns near Coulomb-barrier energies could provide a detailed probe of the potential in the nuclear surface region. (The potential in the nuclear interior is probably inaccessible because of the strong absorption.) One may speculate that the potential for a deformed nucleus may exhibit irregular variations with polar angle β. For example, the imaginary potential may be largely due at barrier energies to loss of flux into neutron transfer channels, and hence be strongest in the zones of the lightly-bound Nilsson neutron orbitals. If the concept of a classical trajectory has any physical significance in these heavy-ion systems, excitation of different states should probe different angular regions of the nuclear surface. Referring to fig. 5, we would infer that the excitation probability for spin 8 in the case displayed there mainly probes the nuclear potential near $\beta = 20^0$, since the large-angle root β_2' feels less influence from the nuclear potential. Excitation of lower spins should be sensitive to regions closer to the nuclear tips. At sufficiently higher energies the low-angle roots should be damped [Cf. fig. 10] and the larger-angle orientations, which now feel the nuclear force, should make the dominant contribution. Therefore, one would expect the probabilities in this case to be sensitive to the nuclear potential nearer the belly of the classical nucleus.

As another example, significant attention has recently been directed to the possibility of different charge and matter distributions in the nucleus.[7] Since the calculations discussed here are very sensitive to the competition between the nuclear forces (arising from the matter distribution) and electromagnetic forces (arising from the charge distribution),

rotational excitation in the surface region could also provide an indication of different charge and mass deformations, if such effects actually occur.

It would be premature to attempt a detailed theoretical exploration of potentials with more parameters representing irregular angular dependence, or differing charge and matter distributions. There are few data available yet, and only experimental data can ascertain whether the effects discussed here are measurable. However, these considerations at least indicate that detailed information about the deformed nuclear potential in the surface region may be available in the Coulomb-nuclear interference experiments suggested by these calculations.

With heavy ions the resolution of different rotational states by traditional charged-particle spectroscopy is presently difficult or impossible. The most promising source of the rotational probabilities for very heavy ions is γ-ray spectroscopy of the rotational-band cascade in coincidence with scattered particles. In Fig. 13 we show for potentials I, II and III the summed intensities that one would expect to see for several states in such a cascade (potential IV is omitted because it is very similar to III). Although there are still obvious differences in the potentials, the detailed structure of Figs. 11 and 12 is quickly washed out by the superposition of intensities in the feeding cascade. The excitation probabilities, rather than the summed intensities, are clearly the experimental quantities of greatest interest. These are accessible by difference, however, and can probably be determined with 5-10% uncertainty in careful experiments.

Theoretically it would be advantageous to extend this method to $\ell > 0$ incident partial waves by treating the full three-dimensional rotor explicitly[44] rather than by the geometrical weighting of the two-dimensional rotor discussed here. This would make it possible to study excitation probabilities as a function of scattering angle. Furthermore, for Xe and heavier projectiles it is experimentally very difficult to detect the scattered particles incident with small impact parameter because they have low scattering energies in the laboratory system.

Additional consideration must also be given to the situation where more than two trajectories contribute to the two-dimensional S-matrix, both for real time paths and for processes accomplished by complex time paths during the period of interaction. Preliminary investigations with direct integration methods similar to those of ref. 24, and with complex time paths in the present method,[39] suggest that for the cases considered here no more than two trajectories make significant contributions to the S-matrix. For some nuclear potentials and for some bombarding energies this may no longer be true, and it may be necessary to consider more than two contributions to the S-matrix.[39] The additional complications arising in such a situation are related to the problems investigated in refs. 21, 45-46. The calculations presented here should be sufficient, however, to suggest the amount and type of information available from heavy-ion rotational inelastic scattering at barrier and sub-barrier energies.

ACKNOWLEDGMENTS

We would like to thank a large number of colleagues for useful and enlightening discussions, including Drs. J. P. Boisson, A. Bohr, J. Vary, F. Videback, I. Y. Lee, A. Winther, W. Miller, and R. Malfliet. We also thank Drs. R. Vandenbosch and J. Birkelund for communicating nuclear potentials prior to publication.

FOOTNOTES AND REFERENCES

*Operated by the University of California for the U.S. Energy Research and Development Administration.

†Present address: Hahn-Meitner Institut für Kernforschung, Berlin, W. Germany. On leave from Facultad de Ciencias, Universidad de Chile, Santiago, Chile.

1) M. Samuel and V. Smilansky, Phys. Lett. 28B (1968) 318.

2) R. J. Pryor, F. Roesel, J. X. Saladin, and K. Alder, Phys. Lett. 32B (1970) 26.

3) W. Brückner, J. G. Merdinger, D. Pelte, V. Smilansky, and K. Traxel, Phys. Rev. Lett. 30 (1973) 57.

4) C. E. Bemis, Jr., P. H. Stelson, F. K. McGowan, W. T. Milner, J. L. C. Ford, Jr., R. L. Robinson, and W. Tuttle, Phys. Rev. C8 (1973) 1934.

5) I. Y. Lee, J. X. Saladin, C. Baktash, J. E. Holden, and J. O'Brien, Phys. Rev. Lett. 33 (1974) 383.

6) A. H. Shaw and J. S. Greenberg, Phys. Rev. C10 (1974) 263.

7) I.Y.Lee, J.X.Saladin, J.Holden, J.O'Brien, C.Baktash, C.Bemis, Jr., P.H.Stelson, F.K.McGowan, W.T.Milner, J.L.C.Ford, Jr., R.L.Robinson, and W.Tuttle, Phys. Rev. C12 (1975) 1483.

8) W. Brückner, D. Husar, D. Pelte, K. Traxel, M. Samuel, and U. Smilansky, Nucl. Phys. A231 (1974) 159.

9) F. Videbaek, I. Chernov, P. R. Christensen, and E. E. Gross, Phys. Rev. Lett. 28 (1972) 1072.

10) P. R. Christensen, I. Chernov, E. E. Gross, R. Stokstad, and F. Videbaek, Nucl. Phys. A207 (1973) 433.

11) E. E. Gross, H. G. Bingham, M. L. Halbert, D. C. Hensley, and M. J. Saltmarsh, Phys. Rev. C10 (1974) 45.

12) J. L. C. Ford, K. S. Toth, D. C. Hensley, R. M. Gaedke, P. J. Riley, and S. T. Thornton, Phys. Rev. C8 (1973) 1912.

13) Y. A. Glukhov, V. I. Man'ko, B. G. Novatskii, A. A. Ogloblin, S. B. Sakuta, D. N. Stepanov, and V. I. Chuev, Sov. J. Nucl. Phys. 19 (1974) 616.

14) J. O. Rasmussen and K. Sugawara-Tanabe, Nucl. Phys. A171 (1971) 497.

15) P. W. Riesenfeldt and T. D. Thomas, Phys. Rev. C2 (1970) 711, 2448.

16) H. Holm and W. Greiner, Nucl. Phys. A195 (1972) 333.

17) M. W. Guidry, H. Massmann, R. Donangelo, and J. O. Rasmussen, to be published.

18) R. A. Malfliet, Symposium on Classical and Quantum Mechanical Aspects of Heavy Ion Collisions, Heidelberg (1974).

19) T. Koeling and R. A. Malfliet, Phys. Rep. 22C (1975) 182.

20) J. Knoll and R. Schaeffer, Phys. Lett. 52B (1974) 131.

21) J. Knoll and R. Schaeffer, "Semiclassical Scattering Theory with Complex Trajectories, I-Elastic Waves", to be published in Annals of Physics.

22) S. Levit, V. Smilansky, and D. Pelte, Phys. Lett. 53B (1974) 39.

23) H. Massmann and J. O. Rasmussen, Nucl. Phys. A243 (1975) 155; H. Massmann, Ph.D. Thesis, University of California, Berkeley (1975), unpublished.

24) R. Donangelo, M. W. Guidry, and J. O. Rasmussen, submitted to Phys. Lett. B.

25) W. H. Miller, J. Chem. Phys. 53 (1970) 1949.

26) W. H. Miller, J. Chem. Phys. 53 (1970) 3578.

27) W. H. Miller and T. F. George, J. Chem. Phys. 56 (1972) 5668.

28) T. F. George and W. H. Miller, J. Chem. Phys. 57 (1972) 2458.

29) J. D. Doll, T. F. George and W. H. Miller, J. Chem. Phys. 58 (1972) 1343.

30) W. H. Miller, Adv. Chem. Phys. 25 (1974) 69.

31) W. H. Miller, "The Classical S-Matrix in Molecular Collisions", in Molecular Beams, ed. K. P. Lawley, (to be published, 1975, Wiley & Sons)

32) R. A. Marcus, J. Chem. Phys. Lett. 7 (1970) 525.

33) R. A. Marcus, J. Chem. Phys. 54 (1971) 3965.

34) J. N. L. Connor and R. A. Marcus, J. Chem. Phys. 55 (1971) 5636.

35) C. Chester, B. Friedman and F. Ursell, Proc. Cambridge Phil. Soc. 53 (1957) 599.

36) J. N. L. Connor, Mol. Phys. 25 (1973) 181; 26 (1973) 1217; 27 (1974) 853.

37) A. Winther and J. DeBoer, in "Coulomb Excitation", ed. K. Alder and A. Winther (Academic Press, New York), p. 303.

38) R. A. Broglia, S. Landowne, R. A. Malfliet, V. Rostokin, and A. Winther, Phys. Rep. 11C (1974) 1.

39) M. W. Guidry, H. Massmann, R. Donangelo and J. O. Rasmussen, unpublished.

40) C. E. Bemis, Jr., F. K. McGowan, J. L. C. Ford, W. T. Milner, P. H. Stelson, and R. L. Robinson, Phys. Rev. C8 (1973) 1466.

41) D. L. Hendrie, Phys. Rev. Lett. 31 (1973) 478.

42) R. Vandenbosch, T. D. Thomas, and M. Webb, Symposium on Classical and Quantum Mechanical Aspects of Heavy Ion Collisions, Heidelberg (October, 1974).

43) J. R. Birkelund, J. R. Huizenga, H. Friesleben, K. L. Wolf, and J. P. Unik and V. E. Viola, Jr., Phys. Rev. C13 (1976) 133.

44) P. Fröbrich, Q. K. K. Liu, and K. Möhring, submitted to Phys. Rev. C, and to be published.

45) S. Landowne, C. H. Dasso, B. S. Nilsson, R. A. Broglia, and A. Winther (to be published).

46) H. Massmann, P. Ring and J. O. Rasmussen, Phys. Lett 57B (1975) 417.

TABLE 1. The parameter sets used in the calculation.

	I	II[c]	III[d]	IV[e]
Q_2 (eb)[a]	11.12	11.12	11.12	11.12
Q_4 (eb^2)[a]	1.96	1.96	1.96	1.96
V_0 (MeV)	0	50.0	73.0	17.7
a_R (fm)	0	0.95	0.624	0.531
R_0^R (fm)	0	1.167	1.131	1.267
W_0 (MeV)	0	2.0	80.3	15.4
a_I (fm)	0	0.28	0.624	0.531
R_0^I (fm)	0	1.305	1.131	1.267
β_2[b]	0	0.237	0.237	0.237
β_4[b]	0	0.067	0.067	0.067

[a]From ref. 40.

[b]From ref. 41.

[c]Nuclear parameters from ref. 42

[d]Nuclear parameters from ref. 43.

[e]Nuclear parameters from ref. 43.

Fig. 1. The coordinate system used in the calculations.

Fig. 2. The classical model for competition between the electromagnetic and nuclear forces.

Fig. 3. The real and imaginary parts of the Coulomb and nuclear potentials of Table 1 as a function of the real part of the radial coordinate r.

Fig. 4. The effect of increased nuclear-potential influence on the final classical angular momentum. The radial coordinate is plotted at the top of each graph, and the time of closest approach is indicated by an arrow. The time is in dimensionless units of the time necessary to cover half the distance of closest approach at initial asymtotic velocity.

Fig. 5. The real part of the final spin vs. the real part of the initial orientation angle - the real quantum number function. For the complex trajectory case the function is complex. The effect of the real nuclear potential is to lower the final spin relative to the case of no nuclear potential. Graphical solutions to (8a) for the 10+ state are indicated for the Coulomb excitation case (β_1 and β_2), and the Coulomb-nuclear case (β_1' and β_2'), when the imaginary potential can be ignored.

Fig. 6. Excitation probabilities for $^{40}Ar + ^{238}U$ at E_{lab} = 180 MeV for pure Coulomb excitation (parameter set I) and for nuclear parameter set II.

Fig. 7. The real part of the phase difference $\Delta\Phi$ and the probability amplitudes $\sqrt{p_j}$ for Eq. (13) as a function of final spin for

$^{40}Ar + ^{238}U$ at E_{lab} = 180 MeV using parameter sets I (Coulomb excitation) and II (Coulomb-nuclear excitation). For $I \gtrsim 12$ only one probability amplitude contributes appreciably and it is exponentially damped by the imaginary phase (see eq. 13 and ref. 23).

Fig. 8. The real part of the phase difference $\Delta\Phi$ as a function of energy for $^{40}Ar + ^{238}U$ using parameter sets I (Coulomb excitation) and II (Coulomb-nuclear excitation).

Fig. 9. The variation of rotational excitation probabilities as a function of the radius parameter R_0^R in a purely real potential for $^{40}Ar + ^{238}U$ at E_{lab} = 200 MeV. For this calculation V=50 MeV, a=0.75 fm, and W=0.

Fig. 10. The effective imaginary potential as a function of time for $^{40}Ar + ^{238}U$ at E_{lab} = 205 MeV. Parameter set II has been utilized and several different initial orientations are indicated. The time is parametrized in dimensionless units of the time necessary to cover half the distance of closest approach at initial asymptotic velocity.

Fig. 11. Excitation functions for the 0^+ state in the reaction $^{40}Ar + ^{238}U$. The parameter sets used are listed in Table 1 and the calculation was restricted to the zero impact parameter case.

Fig. 12. Excitation functions for the $2^+ - 12^+$ states in the reaction $^{40}Ar + ^{238}U$. The parameter sets used are listed in Table 1 and the calculation was restricted to the zero impact parameter case.

Fig. 13. The γ-ray intensities expected for some states in ^{238}U excited by ^{40}Ar projectiles. The intensities are summed probabilities for the state and the states feeding it. The parameter sets used in the calculation are listed in Table 1 and all calculations were restricted to zero impact parameter.

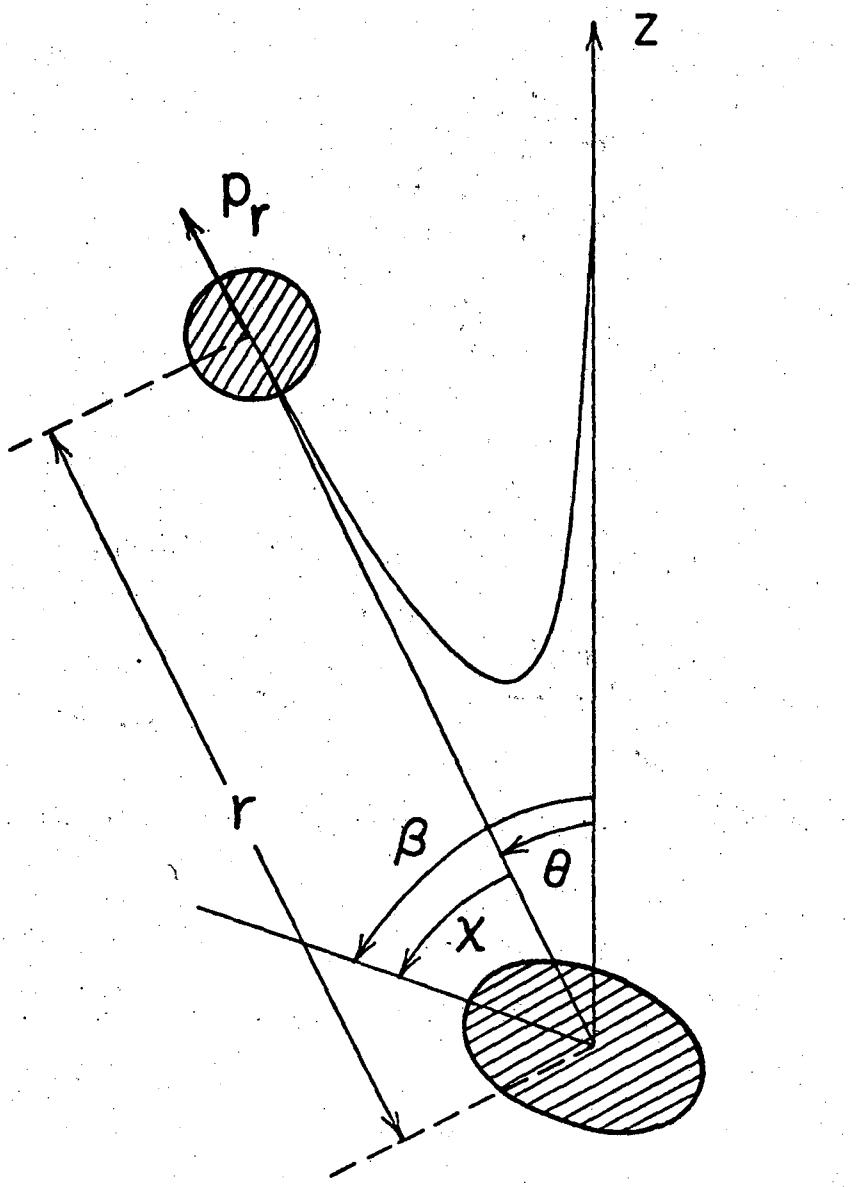

XBL7411-8214

Fig. 1

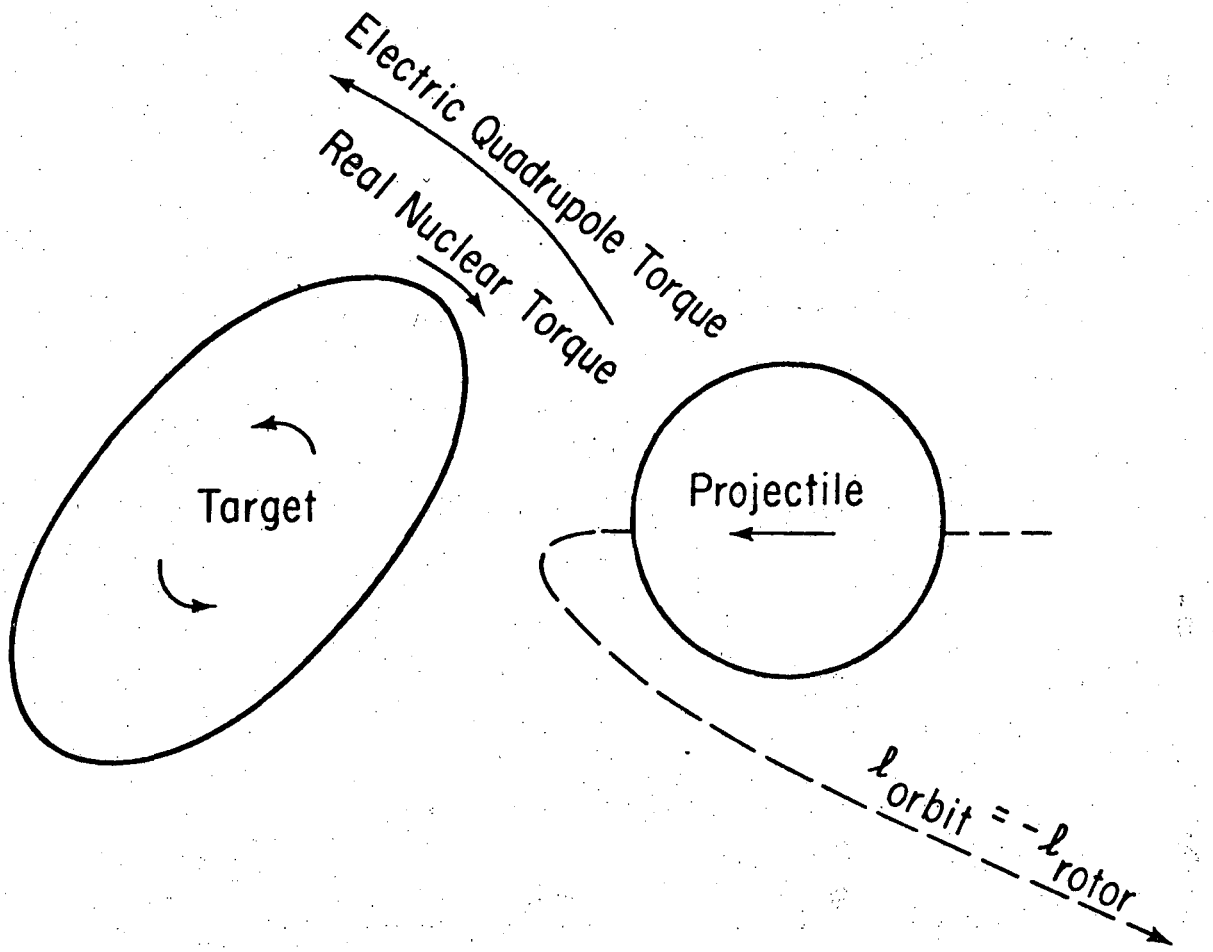
Electric Quadrupole Torque
Real Nuclear Torque
Target
Projectile
$\ell_{orbit} = -\ell_{rotor}$
XBL 761-12A

Fig. 2

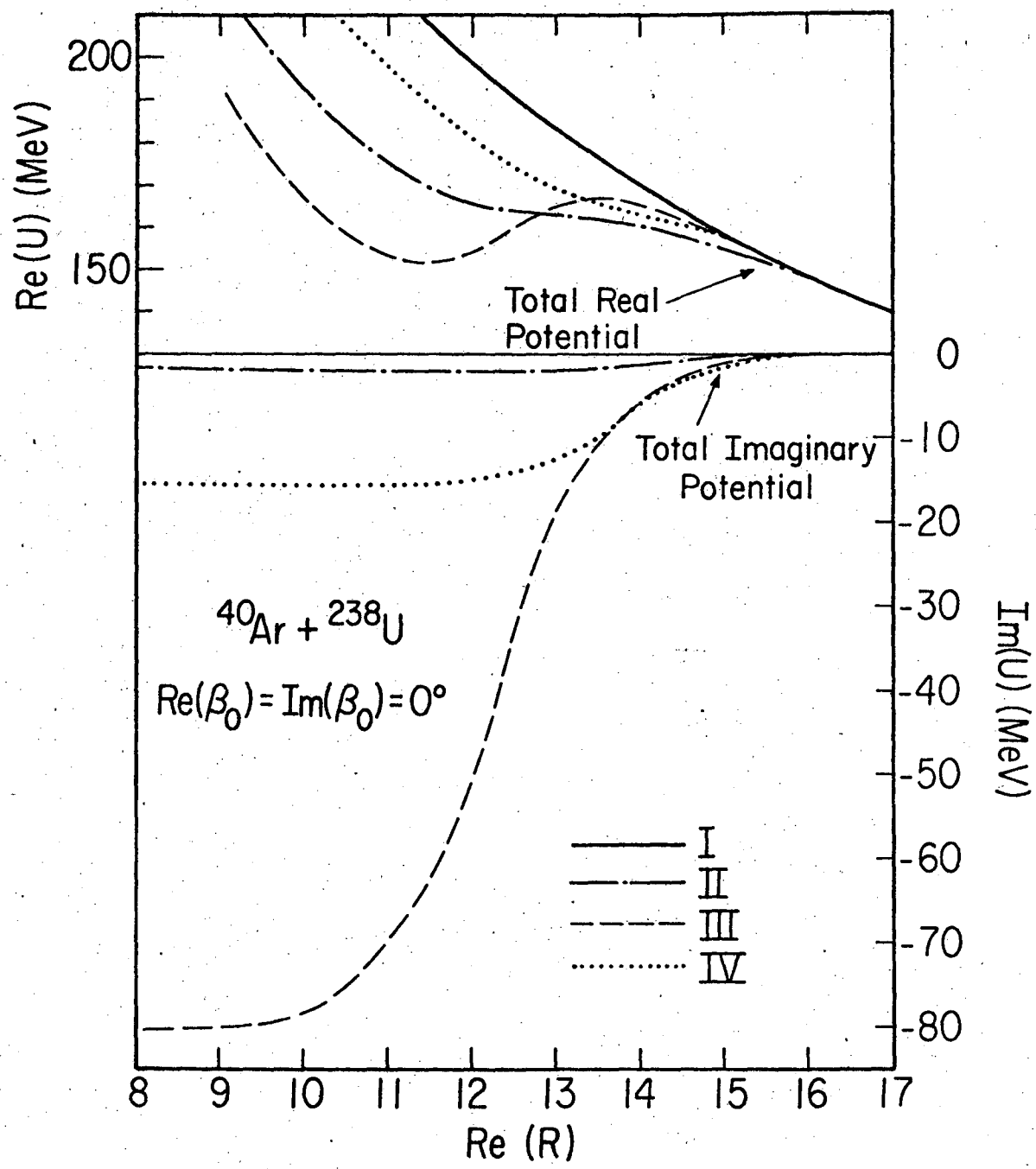

Fig. 3

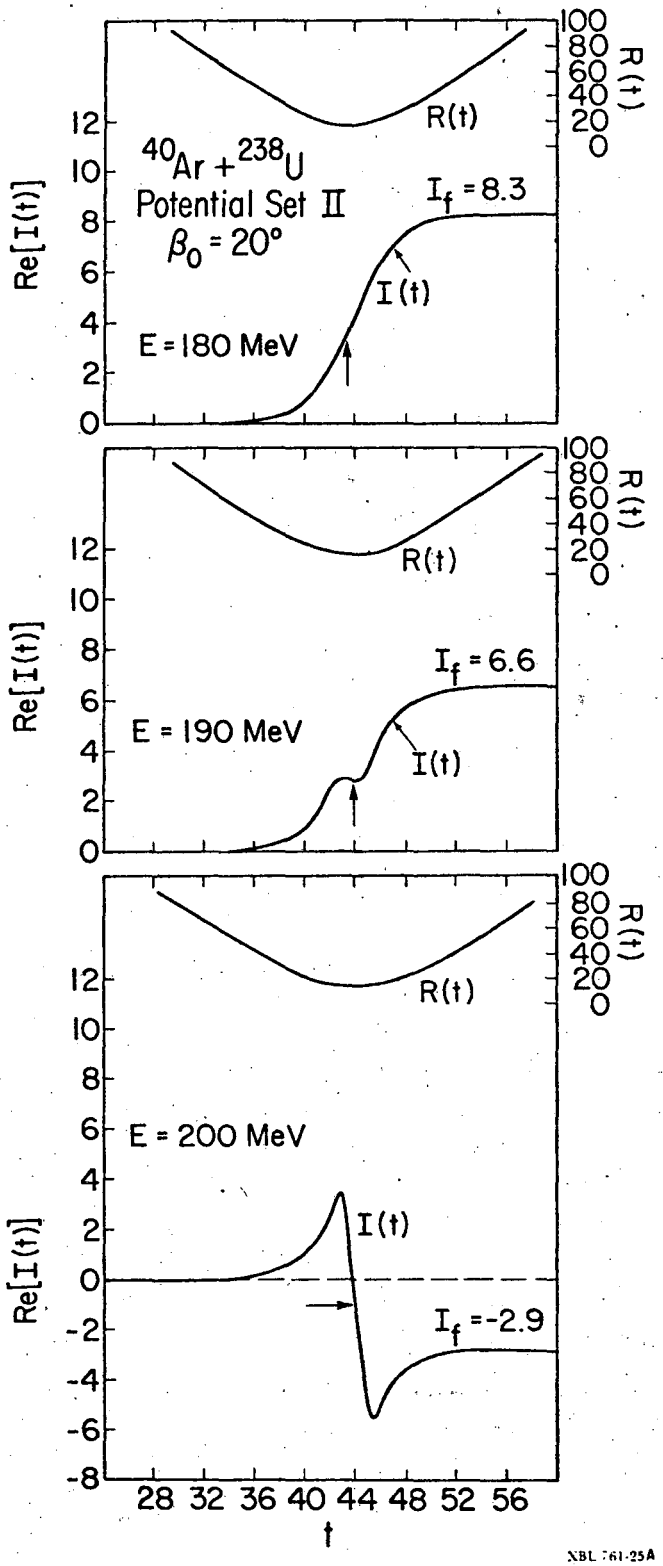
$^{40}Ar + ^{238}U$
Potential Set II
$\beta_0 = 20°$
E = 180 MeV
$I_f = 8.3$
I(t)
R(t)
E = 190 MeV
$I_f = 6.6$
E = 200 MeV
$I_f = -2.9$
Re[I(t)]
R(t)
t
XBL 761-25A

Fig. 4

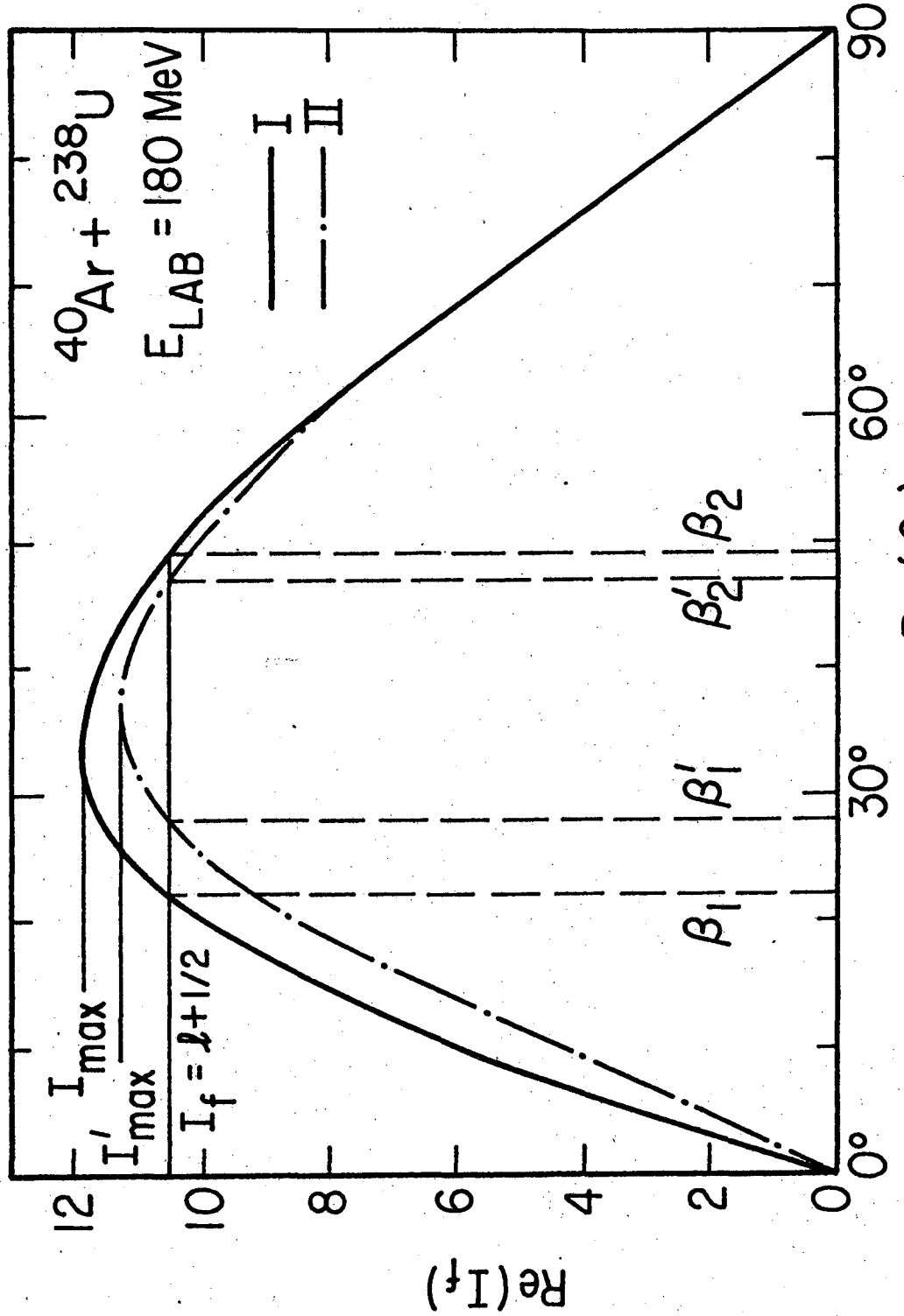

XBL 761-20

Fig. 5

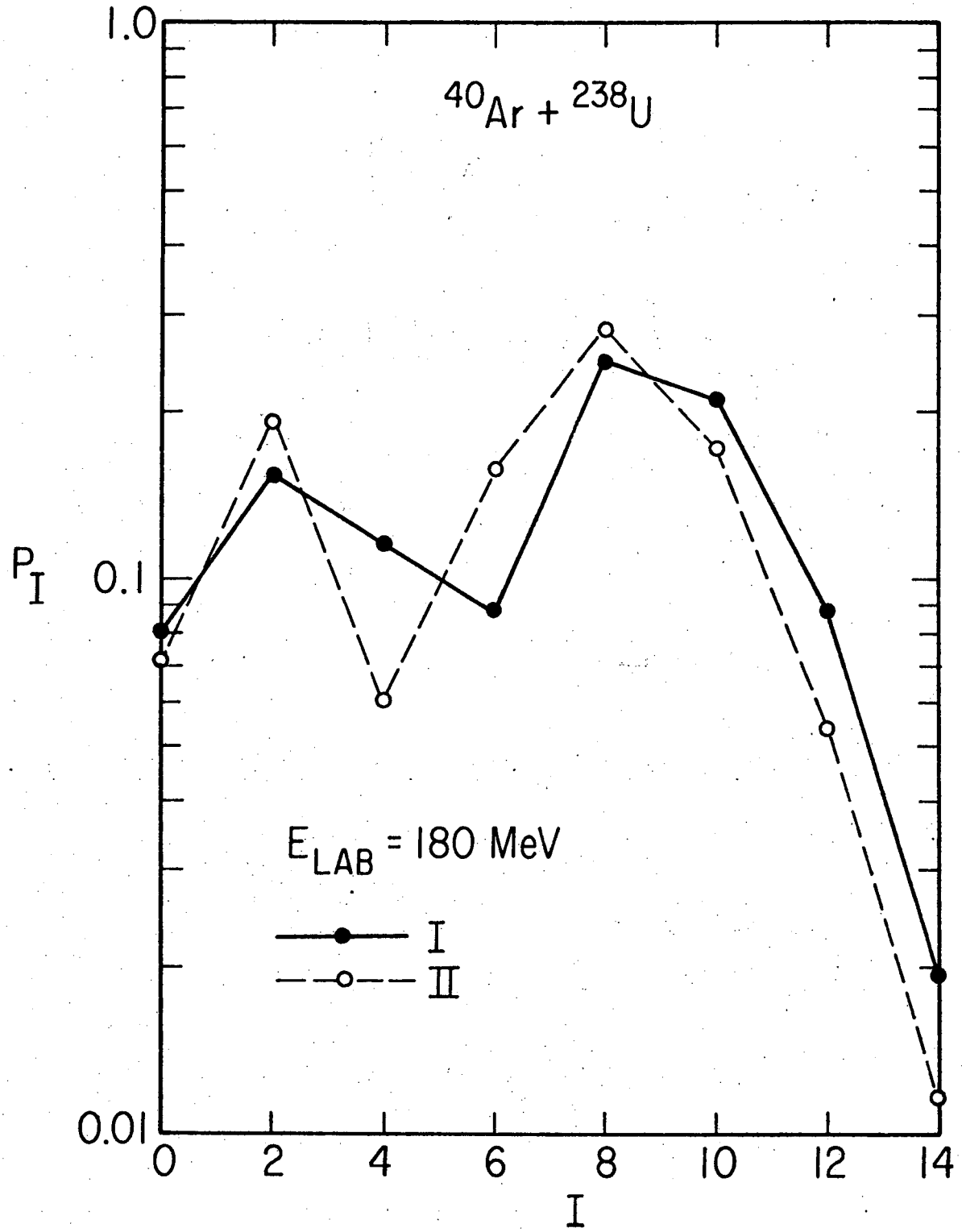

XBL 761-24

Fig. 6

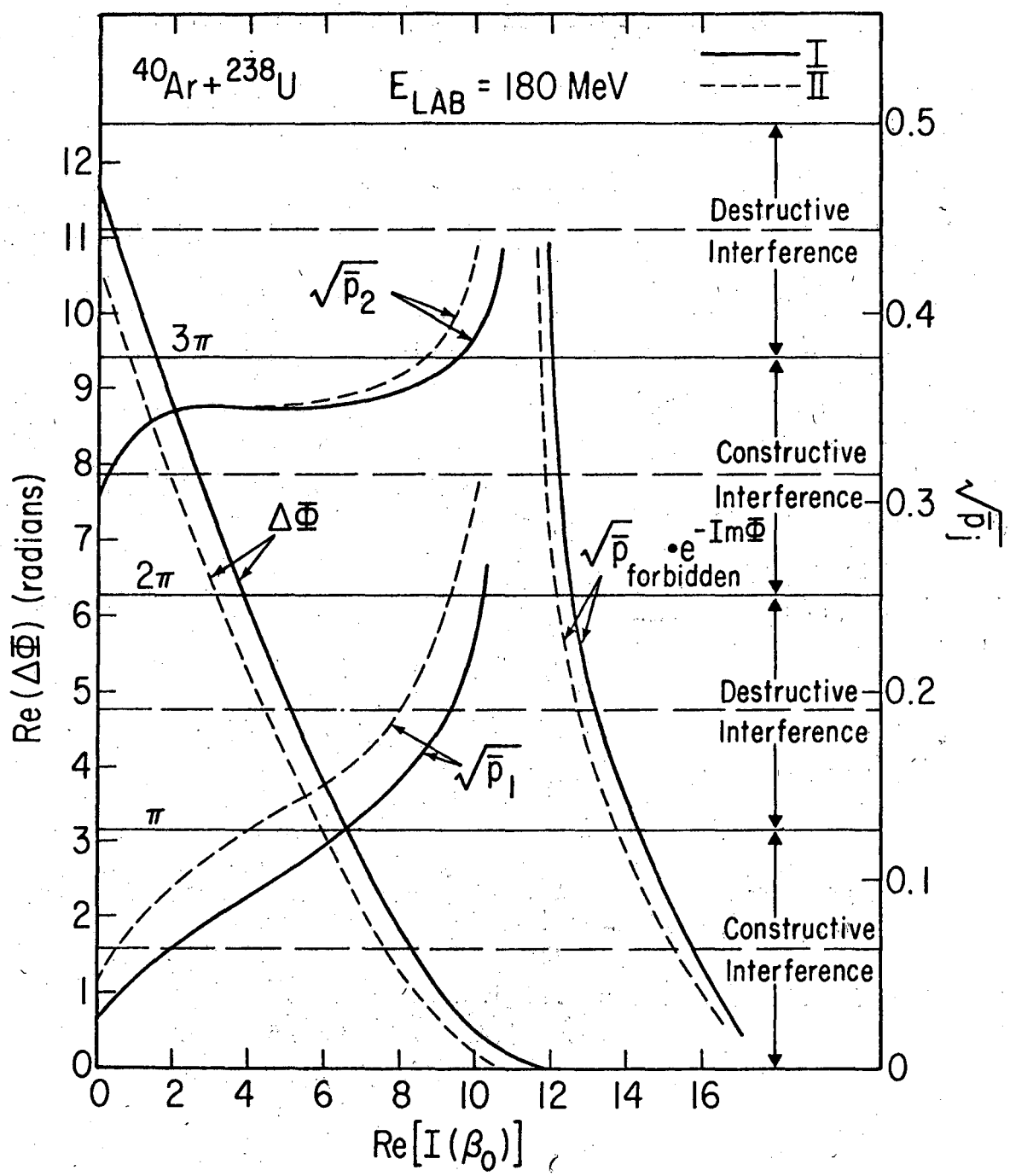

XBL 761-22

Fig. 7

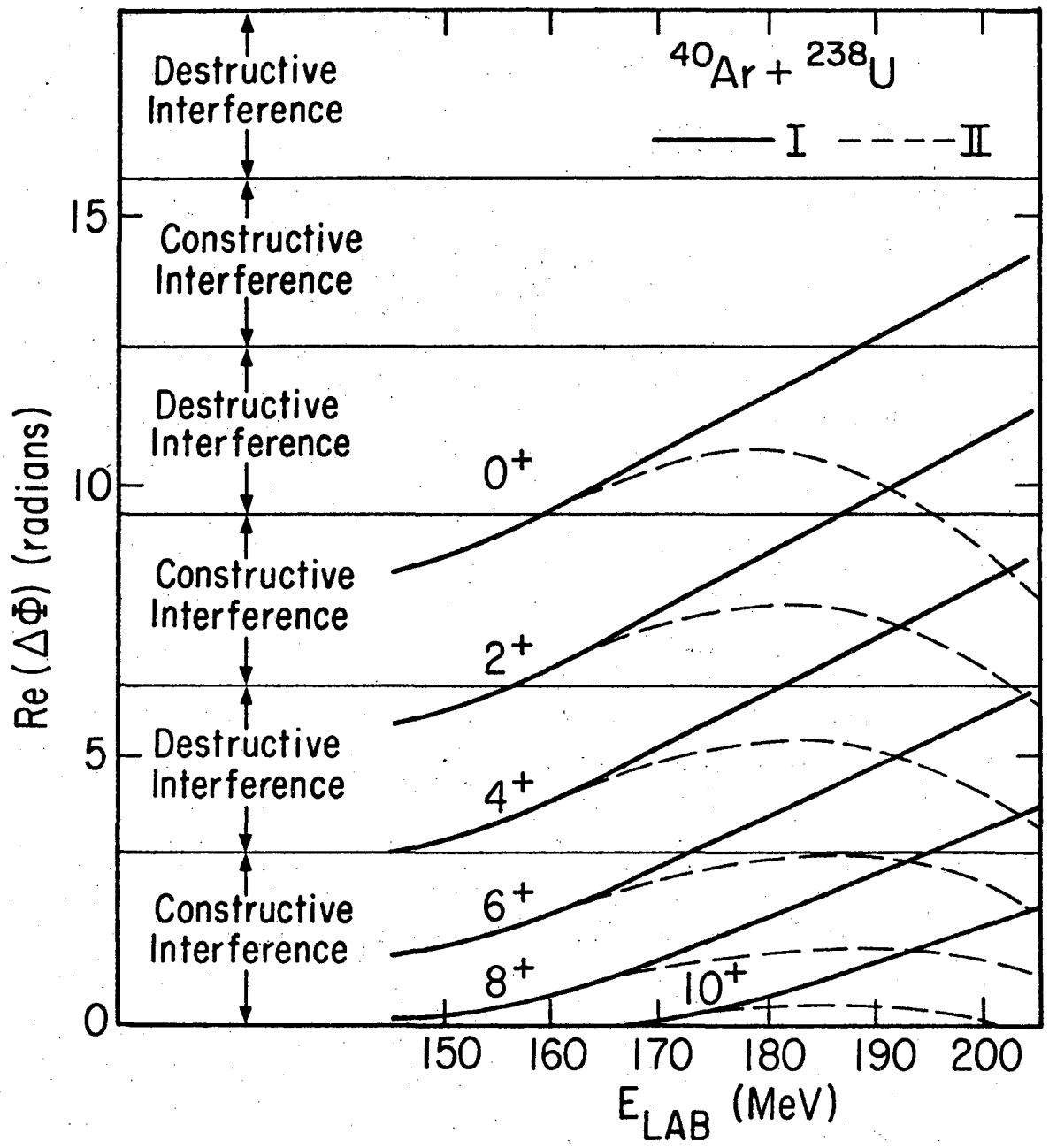

XBL 761-11

Fig. 8

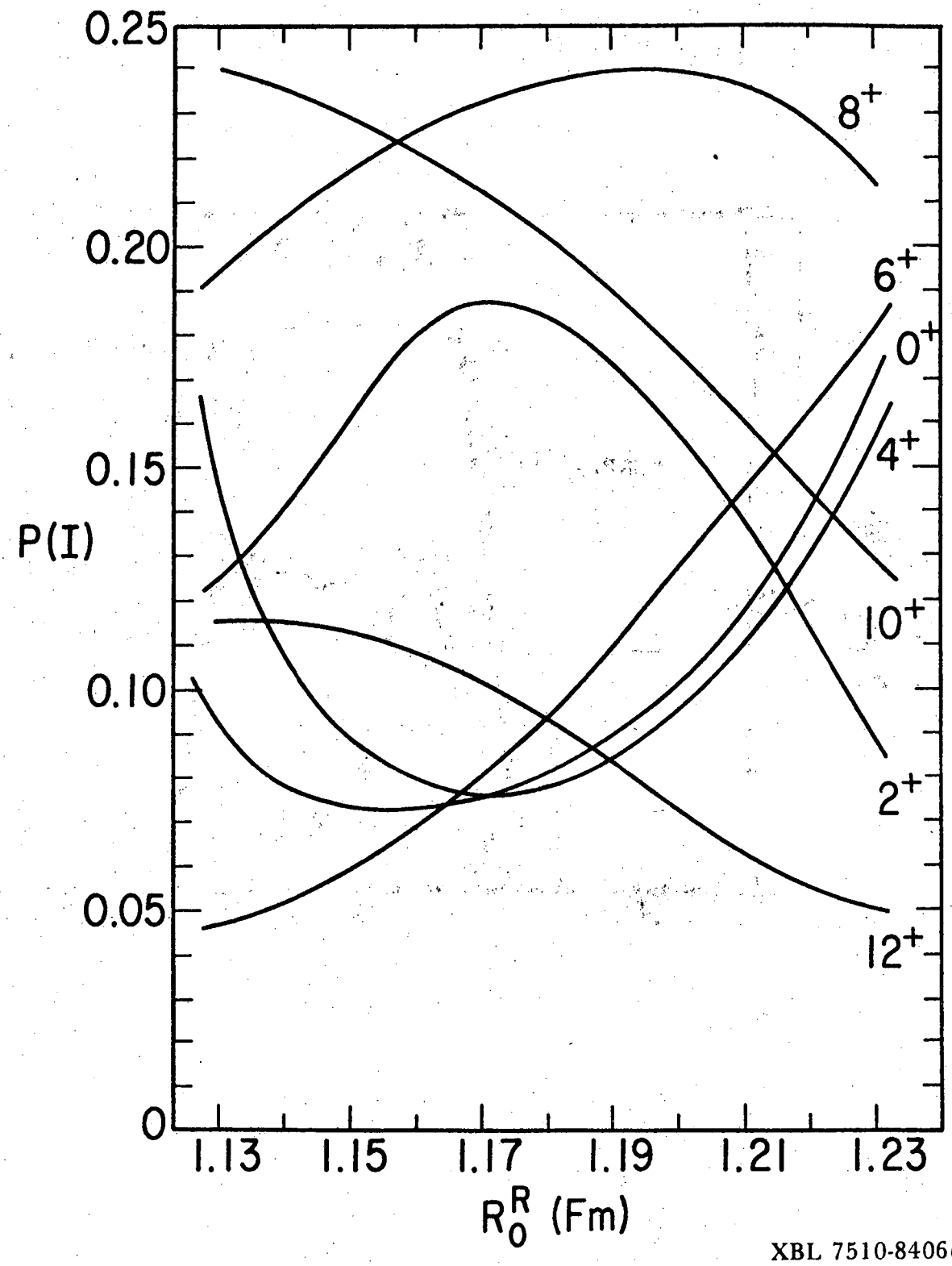

XBL 7510-8406a

Fig. 9

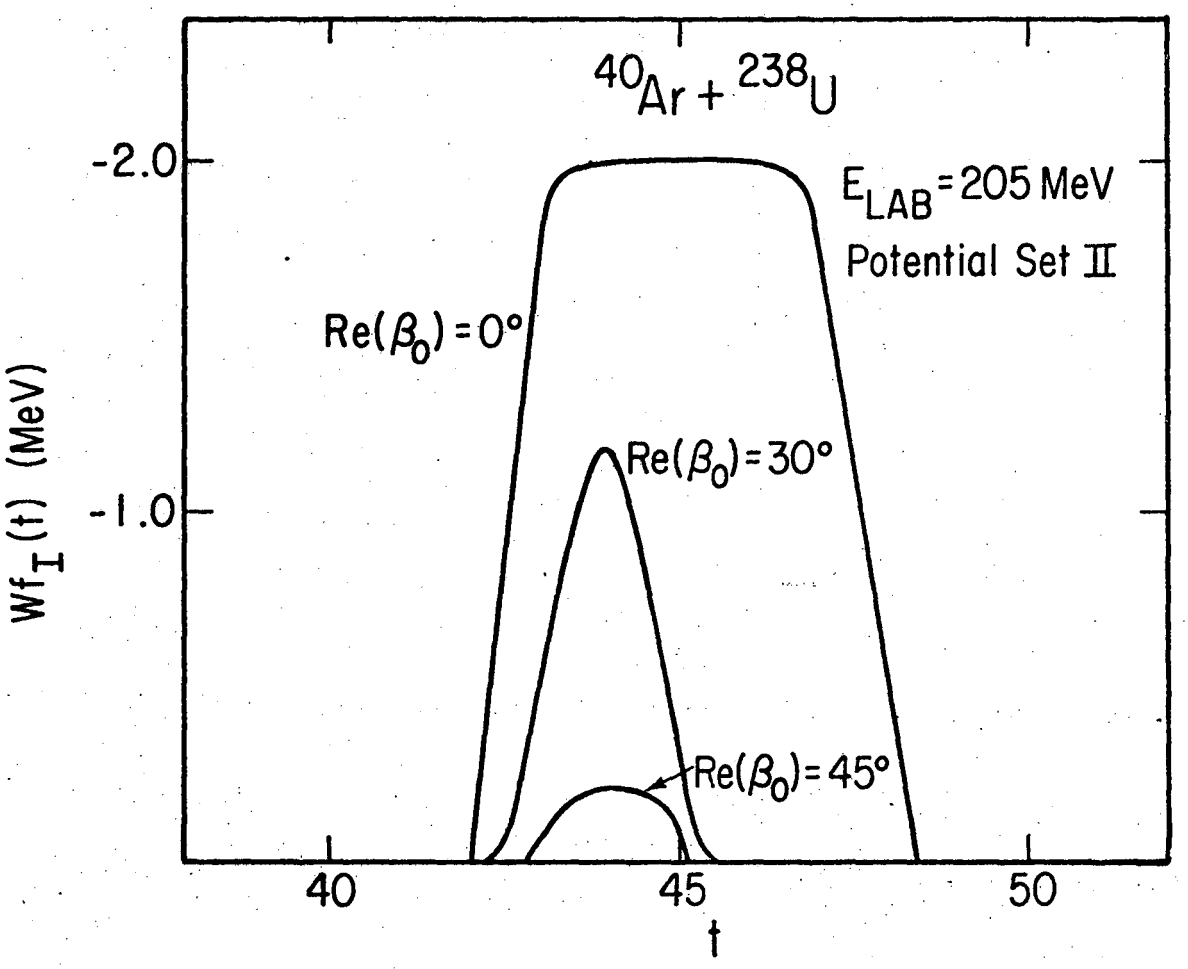

XBL 761-21A

Fig. 10

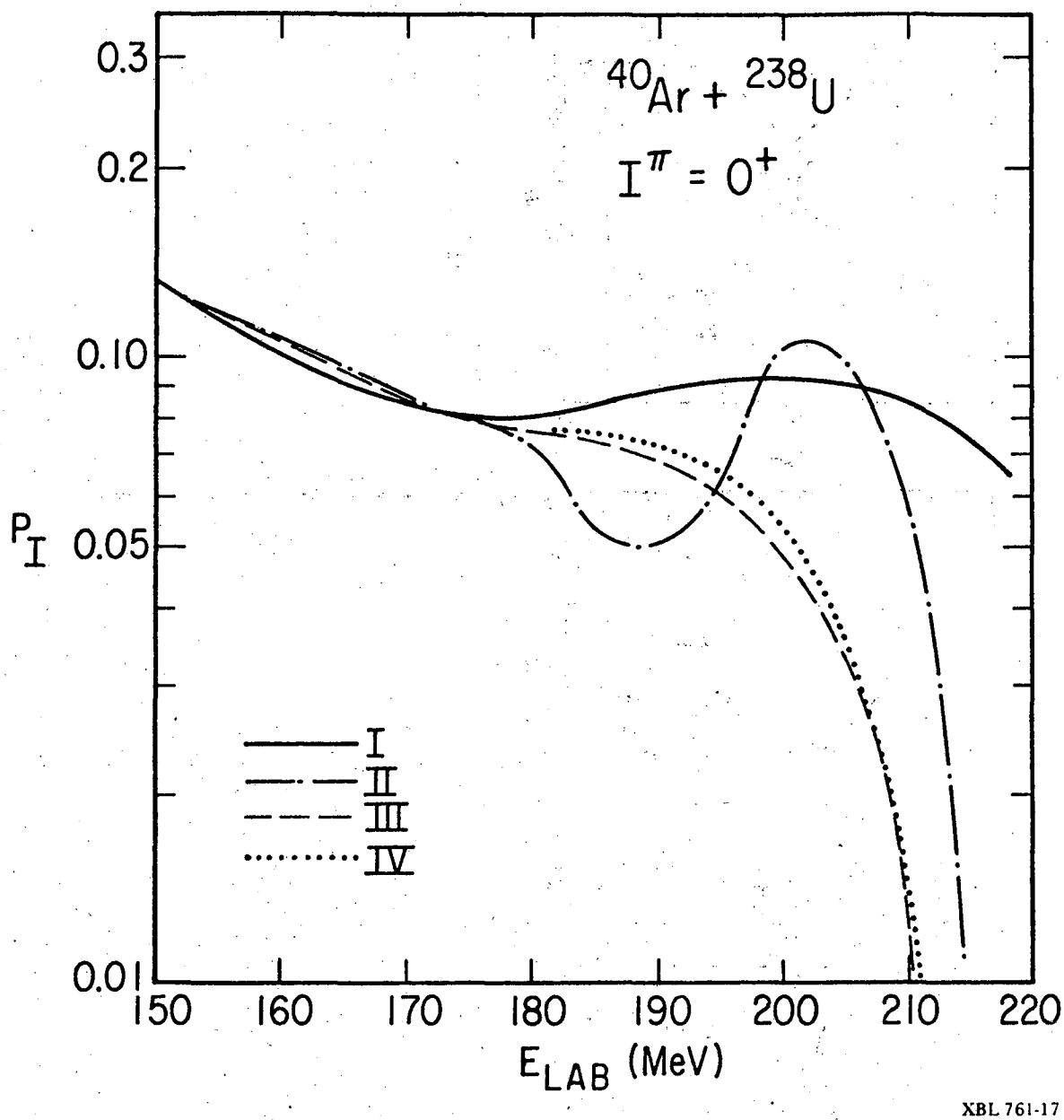

XBL 761-17

Fig. 11

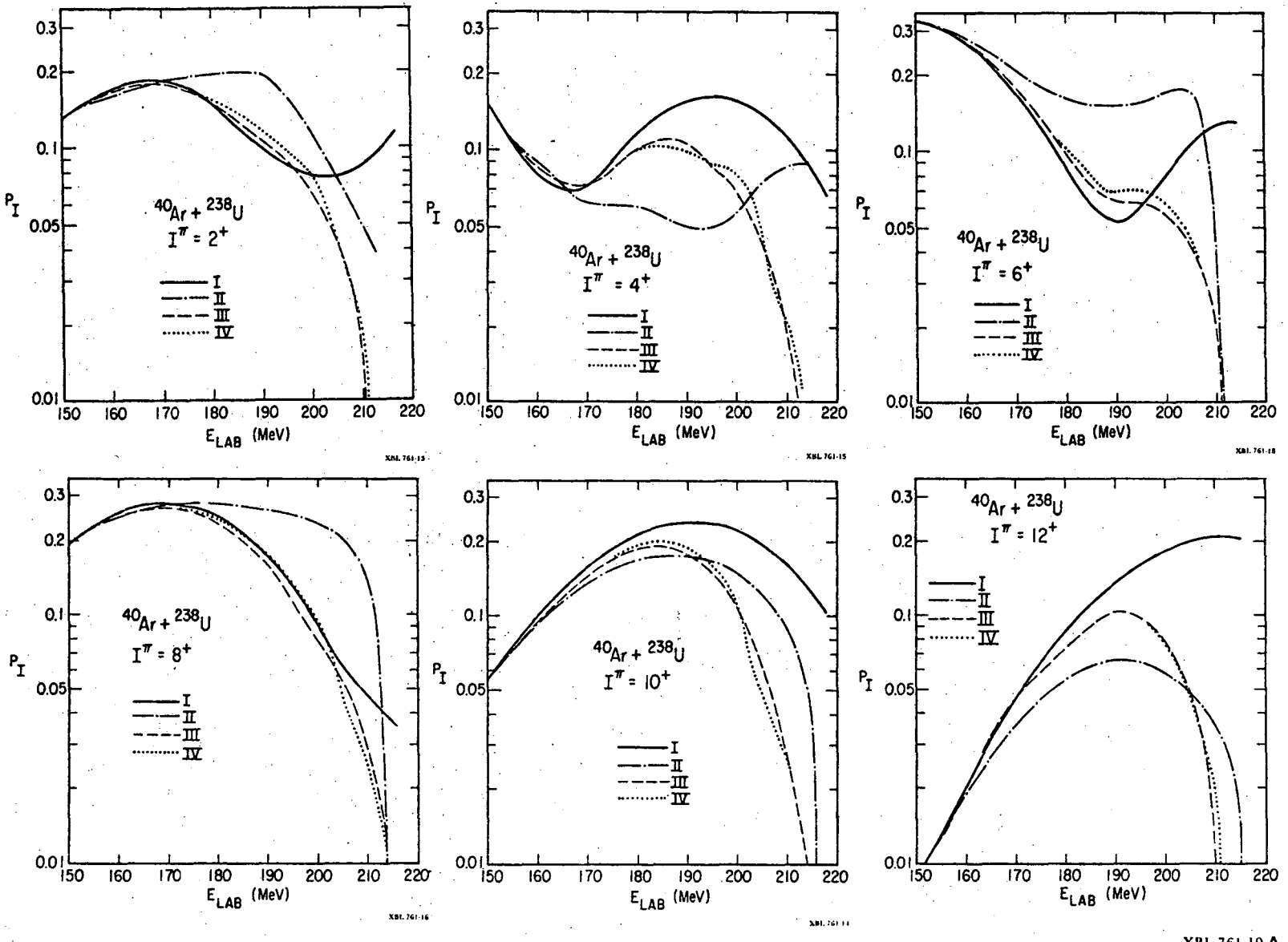
$^{40}Ar + ^{238}U$
$I^{\pi} = 2^+$
$I^{\pi} = 4^+$
$I^{\pi} = 6^+$
$I^{\pi} = 8^+$
$I^{\pi} = 10^+$
$I^{\pi} = 12^+$
I
II
III
IV
P_I
E_{LAB} (MeV)
XBL 761-19 A

Fig. 12

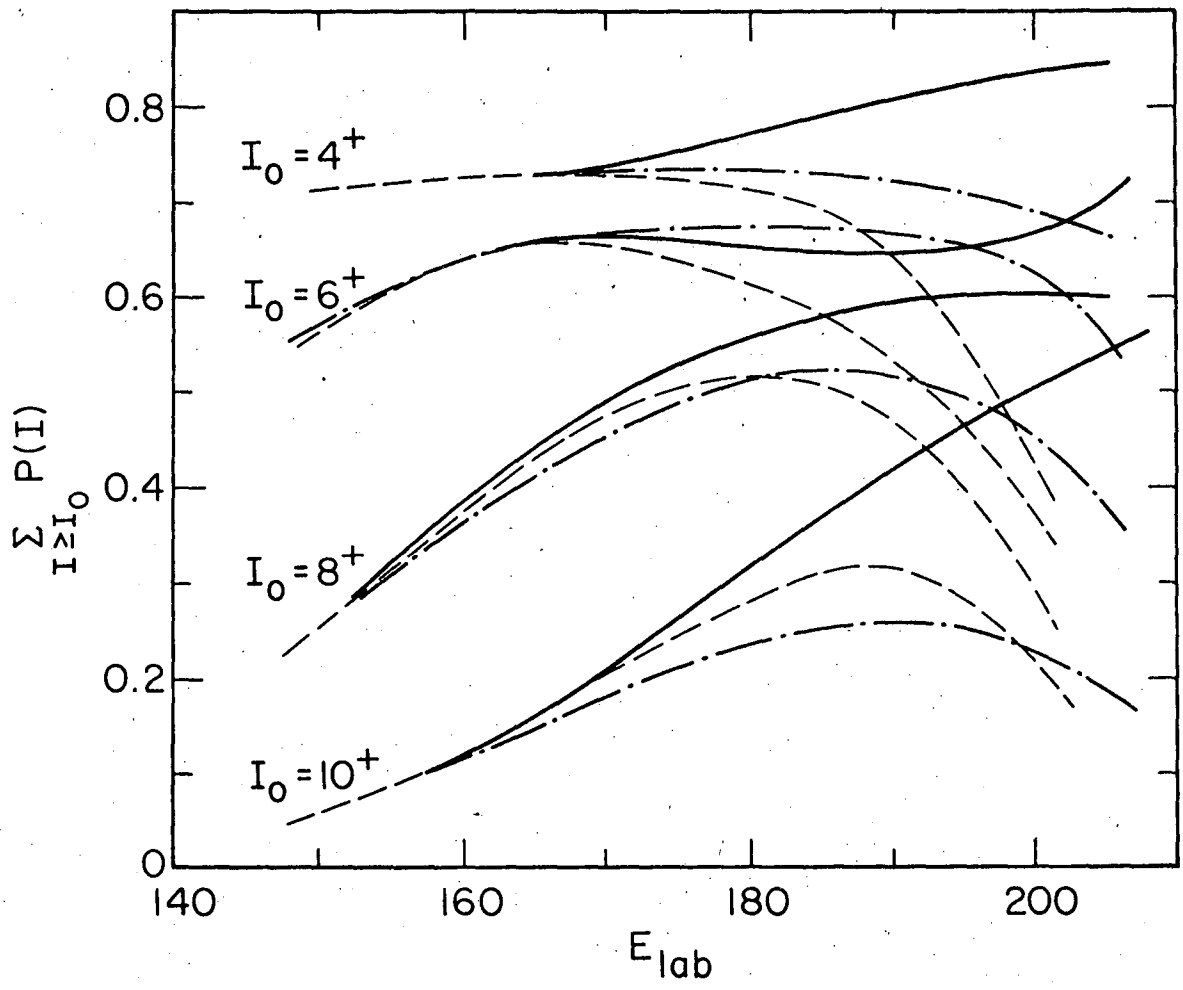

XBL 7510-8407a

Fig. 13

TECHNICAL INFORMATION DIVISION
LAWRENCE BERKELEY LABORATORY
UNIVERSITY OF CALIFORNIA
BERKELEY, CALIFORNIA 94720